PHOTOEXCITATION OF NILE BLUE DYE IN AQUEOUS SOLUTION: TD-DFT STUDY

Kostjukov V.V.[1], Leontieva S.V.[2], Savchenko E.V.[1], Rybakova K.A.[1], Voronin D.P.[1]
[1] Sevastopol State University
Universitetskaya st., 33, Sevastopol, 299053, Russia; e-mail: Viktor_Kostukov@mail.ru
[2] Black Sea Higher Naval Orders of the Red Star School named after P.S. Nakhimov
Dybenko st. 1a, Sevastopol, 299028, Russia
Received 12.07.2022. DOI: 10.29039/rusjbpc.2022.0505

Abstract. The vibronic absorption spectra of Nile blue (NB) oxazine dye in an aqueous solution using 13 hybrid functionals, the 6-31++G(d,p) basis set, and the IEFPCM solvent model were calculated. It turned out that the O3LYP functional provided the best agreement with the experiment. Various parameters of the NB cation in the ground and excited states (IR spectra, atomic charges, dipole moments, and transition moment) were obtained. Maps of the distribution of electron density and electrostatic potential have been built. The influence of four strong hydrogen bonds of the dye with water molecules on the absorption spectrum was analyzed. It has been shown that two from these bonds were strengthened upon NB excitation and two ones were weakened. It was found that explicit assignment of water molecules strongly bound to the dye leads to a redshift of the spectrum as a whole and worsened its shape.
Key words: *TD-DFT, vibronic transitions, aqueous solution, Nile blue, absorption spectrum.*

INTRODUCTION

The Nile blue (NB, Fig. 1) is a highly fluorescent oxazine dye (see reviews [1,2]). The NB was firstly synthesized by Möhlau and Uhlmann in 1896 together with the Nile red (NR) [3].

In the NB molecule, the diethylamino group is an electron donor, and the amino group is an acceptor. The latter contains the positive single charge of the NB molecule. In contrast to electrically neutral NR, the solubility and fluorescence intensity in the water of positively charged NB is much higher. As in the case of NR, the optical properties of an NB depend significantly on its environment. In particular, the absorption and emission maxima of NB also have a redshift (bathochromic) with increasing solvent polarity [1,2]. This positive solvatochromism indicates a greater stabilization of the excited state of the NB molecule by the more polar solvent in comparison with the ground state. Consequently, the magnitude of the dipole moment of NB in the excited state should be greater than in the ground state [4]. However, unlike neutral NR, the positive charge of the NB determines the dependence of its spectral characteristics on pH as well [5]. Besides, the NB molecule is capable of uptake an electron from the solvent and giving it a proton [6]. The spectrophotometrically determined ionization constant of NB in water is pK_a=3.1 [7]. Due to the low sensitivity of NB to small changes in pH, it is recommended to use NB derivatives for its measurement [8]. Therefore, NB is used as a reference signal when measuring pH with the more sensitive FITC [9].

NB forms non-covalent complexes with nucleic acids (both by intercalation and by binding to the minor groove). In the complexes, the NB fluorescence is quenched. This allows it to be used to determine the concentration of nucleic acids. The study of the binding of the NB to DNA was performed by optical [10-14] and electrochemical methods [15-18]. The NB and its derivatives are used as DNA-sensitizing drugs for the photodynamic therapy of cancer [10,19-21] and bacterial [22] diseases. The main mechanism of DNA sensitization is the electron transfer from DNA to NB [11,23,24]. The optical absorption spectrum of the complex of NB with DNA was modeled in Ref. [24] considering this process by the TD-DFT method.

Spectrophotometric studies of NB aggregation on clay sheets [25] showed that NB molecules are capable of forming both J- and H-aggregates. The aggregation of NB in water and an aqueous solution of urea was investigated using adsorption spectrophotometry and interpreted within the framework of the exciton theory in Ref. [26]. The thermodynamics of NB dimerization in water was studied spectrophotometrically [27-31] and using NMR [32]. Aggregation of NB is enhanced by its interaction with colloidal suspensions of SiO_2 and SnO_2 [33], bile salts [34], and single-stranded nucleic acid molecules [12].

NB and its derivatives are used as a fluorescent probe for nanoparticles [35], lysosomes [10,36], proteins [37], protein-ligand complexes [38], micelles [39,40], as well as a Raman detector [41-43]. NB chromophore is a part of sensors [44-47]. The change in the optical characteristics of the NB upon its binding with inorganic compounds is used to detect their traces [48-52]. The NB is also used for optical analysis of the content of anionic surfactants in a sample [53]. The

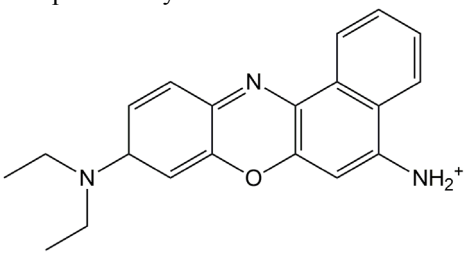

Figure 1. Chemical structure of Nile blue

high photostability of the NB allows it to be used as a laser dye [54] and in solar cells [55]. NB is used in histology and microbiology: its aqueous solution stains acidic components such as phospholipids and nucleic and fatty acids dark blue, while neutral lipids (triglycerides) - pink or red [56,57]. Hydrolysis of the NB produces the NR, which can be used to identify weak fingerprints [58].

Experimental studies of the optical characteristics of the NB were carried out on gold electrodes [59,60], in a monolayer on the surface of quartz glass [61], upon interaction with silver nanoparticles [62], ferrocene [63], graphene oxide [64], quantum dots (fluorescent nanoparticles) [65,66], rhodamine 110 [67] and other objects. Many NB derivatives with improved target characteristics (reduced phototoxicity, increased solubility, stronger luminescence, etc.) have been synthesized [68-72].

A significant number of experimental works are devoted to the study of the optical characteristics of NB itself in various solvents: solvatochromism [5,73-81], absorption [82-86] and emission [87-90] mechanisms, relaxation of excited states [91-94], Raman [95] and two-dimensional electronic (photon echo) [96-99] spectra for the analysis of excited states, nonlinear optical properties [100]. In the context of this work, the experimental results of other authors on solvatochromism and absorption mechanisms are especially interesting for us.

Solvatochromism. In an alkaline aqueous solution (0.1M NaOH or NH_4OH), the heterocyclic nitrogen atom of the NB molecule is hydroxylated, which causes the appearance of a new absorption band with $\lambda_{max}\approx520$ nm (the solution becomes red) [5,73]. In a strongly acidic medium (1M HCl) [5], this nitrogen atom is protonated; the charge of the NB molecule becomes equal to +2 (at low acidity of the solvent, protonation of NB can be photoinduced, i.e., the excited NB molecule undergoes it [74]). This causes a decrease in the intensity of the absorption band with $\lambda_{max}=635$ nm and the appearance of an additional absorption band with $\lambda_{max}=460$ nm (green solution) [5]. In proton-acceptor and electron-donor solvents (aniline, N,N-dimethylaniline, N,N-dimethylaniline) NB under the action of light loses a proton or attaches an electron, while its fluorescence is quenched [6,75-77]. In Ref. [78], based on experimental data, the values of the NB dipole moments in an excited state in various solvents were calculated. As mentioned above, NB exhibits a shift in the absorption and emission maxima to longer wavelengths with increasing solvent polarity. In this case, in the gas phase, they are, respectively, (580±10) nm and (628±1) nm, i.e., less than the corresponding values for most polar solvents, but more than for nonpolar ones [82].

Absorption mechanisms. In Ref. [84], the saturation of the $\pi\rightarrow\pi^*$ the NB transition from the ground to the first excited state ($S_0\rightarrow S_1$) was studied using picosecond laser pulses, at which the transitions to the higher excited states (S_2, S_3, ...) are noticeably reduced. This is accompanied by discoloration of the solution of the NB sulfate in ethanol. An experimental study of the vibronic coupling in the $S_0\rightarrow S_1$ transition using femtosecond laser pulses was performed in Ref. [85].

Theoretical studies of the NB photoexcitation began with the early work of Blanchard [101], in which he calculated the atomic charges of the dye in the ground and excited states using the semiempirical MNDO method. A time-dependent wavepacket theory for dynamic absorption spectroscopy was used to analyze the evolution of the transient absorption spectrum of NB (without considering the solvent) following excitation with a 6 fs pulse in Ref. [102]. In Ref. [103], the energy of the $S_0\rightarrow S_1$ transition in the NB molecule was calculated using the CIS quantum-chemical method (also without accounting for the solvent). Theoretical calculations of the absorption maxima using the TD-DFT vertical transition model with an implicit considering of the aqueous environment (CPCM approach [104]) were carried out in Refs. [81,105]. In Ref. [106], the effect of the solvent and a thermal motion was considered explicitly through hybrid QM/MM calculations, and the low-frequency out-of-plane vibrations of the NB chromophore were estimated. However, in all the above-mentioned works, the calculated values of absorption maximum turned out to be significantly less than the experimental one for NB dilute solution in the aqueous solution $\lambda_{max}=634\ldots636$ nm [26,27,29-31,78,79,80]. However, the vertical transition model itself is quite simplified, although it is widespread in the literature (see review [107]). It does not consider the vibronic coupling, and therefore does not allow theoretically reproducing the asymmetric form of the experimental absorption and emission spectra of organic molecules. At the same time, the shape of the spectrum reflects the pattern of the excited states of the molecule and the transitions between them [108].

METHODS

When a photon is absorbed, both the electronic and vibrational energy of the molecule of the dissolved substance in the solution changes, i.e. a vibronic transition occurs in it (Fig. 2). According to the Franck-Condon principle [109], the electronic transition from the ground state (GS) to the excited state (ES) occurs at constant coordinates of the nuclei of the solute molecule, as well as the nuclei of the nearest solvation shell (vertical transition E_{vert} in Fig. 2). In this case, the molecule is in excited nonequilibrium (Franck-Condon, FC) state. This non-equilibrium nuclear core leads to the activation of vibrational energy levels (green wave in Fig. 2). Since the latter obey the Boltzmann distribution, there are many transitions from different vibrational levels of the ground electronic state to different vibrational levels of the electronically excited state.

To calculate the vibronic one-photon absorption spectra, we used a generalized approach [110] implemented in the Gaussian16 software package [111]. This method is a time-dependent extension of time-independent vibronic spectroscopy, in which the intensity of a vibronic transition is calculated as

$$I = \propto \omega \sum_m \sum_n \rho_m \mu_{mn}^2 \, \delta\left(\frac{E_n - E_m}{\hbar} - \omega\right), \quad (1)$$

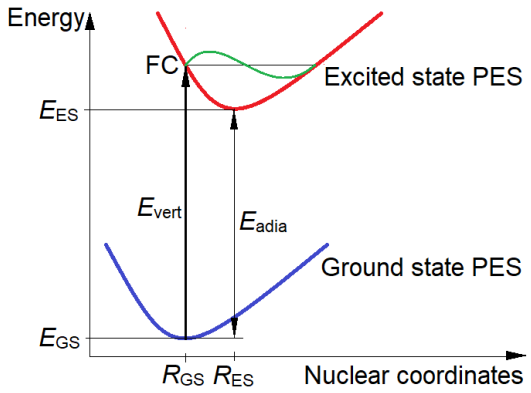

Figure 2. Energetic diagram of vibronic transition

where $\propto = \frac{10\pi N_A}{3\varepsilon_0 \ln(10)\hbar c}$, ω - frequency of the absorbed photon, the summation is performed over all m vibrational levels of the ground state and n vibrational levels of the excited state, ρ_m is the Boltzmann population of vibrational levels of the ground state, μ_{mn} is the transition dipole moment, δ is the Dirac distribution function.

The main problem in Eq. (1) is that the analytical expression for μ_{mn} remains unknown. Therefore, in practice, the Taylor series is used near the equilibrium geometry of the ground electronic state:

$$\mu_{mn}(\boldsymbol{Q}) = \mu_{mn}(\boldsymbol{Q}_{GS}) + \sum_{i=1}^{N} \left(\frac{\partial \mu_{mn}}{\partial Q_i}\right)_0 \boldsymbol{Q}_i + \ldots, \quad (2)$$

where $\boldsymbol{Q}$ are mass-weighted normal coordinates. The zeroth-order term in Eq. (2) corresponds to the Franck-Condon approximation (strong, allowed transitions) [109], and the first-order correction to the Herzberg-Teller approach (weak, forbidden transitions) [112]. To calculate the vibronic spectra, we used the general Franck-Condon-Herzberg-Teller method [113].

Calculation of vibronic spectra requires a calculation of the overlap integrals, which depend on the normal vibrational modes of the ground and excited states. For integration, the Duschinsky linear transformation [114] is used to represent two corresponding sets of coordinates with each other:

$$\boldsymbol{Q}_{GS} = \boldsymbol{J}\boldsymbol{Q}_{ES} + \boldsymbol{K}, \quad (3)$$

where $\boldsymbol{J}$ is the Duschinsky matrix, $\boldsymbol{K}$ is the shift-vector. The expressions for $\boldsymbol{J}$ and $\boldsymbol{K}$ depend on the model of the electronic transition (adiabatic or vertical) and the level of approximation (whether the potential energy surfaces (PESs) of the ground and excited states are taken to be the same (see Fig. 2) or not).

The transition from a time-independent approach to a time-dependent theory is realized by replacing summation over states with integration over time. For this, the Dirac distribution function δ in Eq. (1) is replaced by expression $\delta = \frac{1}{2\pi}\int_{-\infty}^{+\infty} e^{i\omega t}\,\mathrm{d}t$. Ultimately, the absorption spectrum is calculated as the Fourier transform of the trace of the exponential operator:

$$I = \propto' \omega \int_{-\infty}^{+\infty} \chi(t) e^{i(\omega_{adia} - \omega)t}\,\mathrm{d}t \quad (4)$$

where $\propto' = \frac{\propto}{Z}$, $Z = \prod_{i=1}^{N}\left[2\sinh\left(\frac{\hbar\omega_i}{2k_BT}\right)\right]^{-1}$ is the total Boltzmann population of vibrational levels of the ground state, $\omega_{adia} = \frac{E_{adia}}{\hbar}$, E_{adia} is the adiabatic energy (difference between the energies of the ground vibrational states of the ground and excited electronic states, see Fig. 2), $\chi(t)$ is the vibrational wave function. The temperature T=298 K was used. For the numerical integration of Eq. (4), 2^{18} steps and the $\Delta t = 2^{18}\times10^{-17} = 2.62\times10^{-12}$ s time interval were used. For broadening the Gaussians with half-width on half maximum HWHM=600 cm^{-1} were chosen so that the calculated spectra corresponded best to the experimental one.

The spectra were calculated using the adiabatic Hessian model, in which both the ground and excited states are considered on the same ground, and the harmonic PESs are calculated near their equilibrium geometry (R_{GS} and R_{ES}, respectively, in Fig. 2). The first derivatives of the electronic moments of the transition along the coordinates, $\frac{\partial \mu_{mn}}{\partial Q_i}$, were calculated numerically. Force constant matrices were calculated from analytical gradients.

We used the IEFPCM approach [115] which includes an external iteration procedure whereby the Gaussian16 computes the energy in solution by making the solvent reaction field self-consistent with the solute electrostatic potential (the latter being generated from the computed electron density) [116]. The Pople's 6-31++G(d,p) basis set was used. It provides acceptable accuracy with moderate resource consumption [117]. Although some authors [118] argue that diffuse functions should be used at transition energies above 5 eV (less than 250 nm), authors of TD-DFT benchmarks [108,117,119] consider their use mandatory.

It is known that the results of TD-DFT calculations of the excited electronic states of organic molecules are largely determined by the functional used [108,117,119-122]. In the case of significant intramolecular charge transfer, it is recommended to use long-range corrected functionals [123-126], e.g. CAM-B3LYP, LC-ωHPBE, and ωB97XD.

The original spatial structure of the NB molecule was taken from the PubChem database (CID 16939). The aminodiethyl group had an *anti* conformation. The visualization of the computational structures, electron densities, and electrostatic potentials was carried out using the Gaussview software [127].

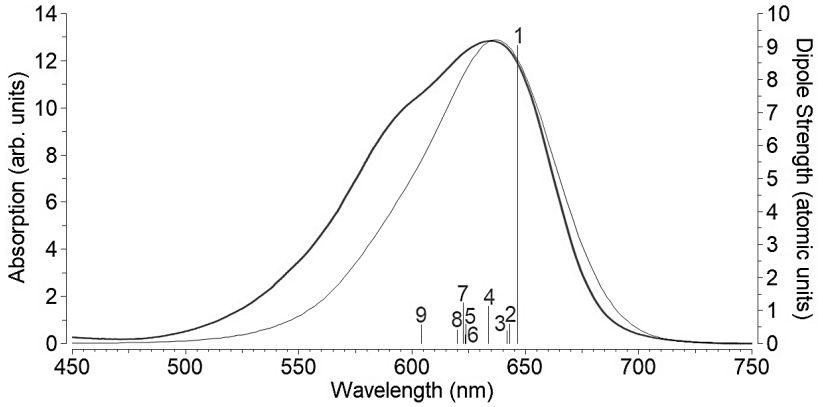

Figure 3. The calculated vibronic absorption spectrum of NB in aqueous solution (thin line) and the corresponding experimental spectrum (2 μM) adapted with permission from Ref. [87] (thick line). Copyright 2001 American Chemical Society. The vertical lines are the dipole strength of the vibronic transitions from Table 2

RESULTS AND DISCUSSION

We analyzed the singlet-singlet transition $S_0 \rightarrow S_1$ (HOMO→LUMO), which determines the absorption of NB in the visible region. The calculated energies of electronic and vibronic transitions largely depend on the fraction X of the exact Hartree-Fock exchange in the functional used. This feature was analyzed in detail in Refs. [121,122]. Therefore, pure functionals with X=0 cannot correctly reproduce the TD-DFT spectra. The vibronic absorption spectrum obtained using the O3LYP [128] functional (X=12 %) with λ_{vibron}=637 nm is in best agreement with the experiment on the position of the maximum λ_{max}≈635 nm (Table 1) and overall shape (Fig. 3). A good result (λ_{vibron}=630 nm) was also shown by the τHCTHhyb functional (X=15 %). Note that the spectrum of a dilute NB solution lacks a short-wavelength shoulder, unlike other oxazine dyes, but asymmetry occurs (the short-wavelength slope is gentler than the long-wavelength one). As can be seen from Fig. 3, this asymmetry is due to vibronic transitions. In addition, one can notice a short-wavelength hump in the experimental spectrum, which has not been reproduced theoretically. Most likely, it is of dimeric origin, since the propensity for NB aggregation is very high [27-32].

O3LYP is an improved version of the most popular B3LYP functional. At the same time, the functionals with long-range correction (CAM-B3LYP, LC-ωHPBE, and ωB97XD) gave λ_{vibron} values that are significantly lower than the experimental λ_{max} value. Table 1 shows that the λ_{vibron} values exceed the vertical transition wavelengths λ_{vert} by ~90 nm. As mentioned in the Introduction, the model of vertical transitions cannot correctly reproduce the experimental spectrum, although a direct comparison of the calculated λ_{vert} and the experimental maximum λ_{max} is widespread in the literature (see Refs. [81,105] for NB). Nevertheless, the comparison between λ_{vibron} and λ_{max} is correct [119]. In the above-mentioned work [105], based on the analysis of the calculated energies of vertical transitions in a series of 10 oxazine dyes, the authors concluded that the CPCM model gives underestimated values of λ_{vert} compared to λ_{max}. They overcame this problem by using the SMD model [129] instead of the CPCM. In this work, this regularity takes place in the case of the of them that ensured the achievement of the experimental λ_{max} value.

The choice of the basis set has a much smaller influence on the calculated vibronic spectrum compared to the functional. In the present study, the differences between the values of λ_{vibron} for different basis sets were insignificant

Table 1. The calculated values of the wavelengths and energies of the vertical transitions and the maxima of the vibronic absorption spectra for NB in aqueous solution (6-31++G(d,p) basis set). For functionals with long-range correction, X for small and large distances are indicated

Functional (X %)	λ_{vert} (nm)	E_{vert} (eV)	λ_{vibron} (nm)	E_{vibron} (eV)
O3LYP (12)	542	2.29	637	1.95
τHCTHhyb (15)	538	2.30	630	1.97
B3LYP (20)	527	2.35	601	2.06
X3LYP (22)	523	2.37	604	2.05
APFD (23)	518	2.39	604	2.05
PBE0 (25)	514	2.41	601	2.06
M06 (27)	519	2.39	599	2.07
SOGGA11X (40)	492	2.52	573	2.16
BMK (42)	490	2.53	541	2.29
M052X (56)	489	2.54	571	2.17
CAM-B3LYP (11-65)	489	2.54	559	2.22
LC-ωHPBE (0-100)	467	2.66	551	2.25
ωB97XD (22-100)	489	2.54	560	2.21

(Table 2). Therefore, further analysis of the NB photoexcitation in an aqueous solution will be performed using the O3LYP/6-31++G(d,p)/IEFPCM theory level.

Comparing the calculated IR spectra of NB in the ground and excited states (Fig. 4), one can see that photoexcitation significantly changes the intensities and the frequencies of the vibrations. The NB cation contains 44 atoms, respectively, the total number of vibrational normal modes is N=3×44-6=126. The intense vibronic transition #7 ($0_0 \rightarrow 34^1$) with ν=597 cm^{-1} is in good agreement with the experimentally observed vibronic mode at ν=590 cm^{-1}, corresponding to deformations of the rings of the NB chromophore [85,86,89,91,96].

According to our calculations, the two next electronic transitions ($S_0 \rightarrow S_2$ and $S_0 \rightarrow S_3$) in the visible region of the spectrum have a very low oscillator strength f (Table 4), and therefore do not make a significant contribution to the absorption spectrum. When calculating the vibronic spectrum of the $S_0 \rightarrow S_1$ transition, the sum of the Franck-Condon factors was 99.69%. Thus, the contribution of the Herzberg-Teller correction in Eq. (2) turned out to be negligible.

Table 2. The calculated values of the wavelengths and energies of the vertical transitions and the maxima of the vibronic absorption spectra for NB in aqueous solution with the O3LYP functional and different Pople's basis sets

Basis set	λ_{vert} (nm)	E_{vert} (eV)	λ_{vibron} (nm)	E_{vibron} (eV)
6-31G(d,p)	542	2.29	636	1.95
6-31++G(d,p)	552	2.25	637	1.95
6-311++G(d,p)	551	2.25	637	1.95
6-311++G(3df,3pd)	548	2.26	637	1.95

Table 3. Calculated parameters of vibronic transitions during NB excitation in an aqueous solution

# (i)	Transition	λ (nm)	ΔE (eV)	ν (cm^{-1})	I	p (a.u.)	Definition of vibrations
1	$0_0 \rightarrow 0^0$	646	1.92	0	76970	9.04	-
2	$0_0 \rightarrow 5^1$	643	1.93	84.9	4929	0.576	Bending vibrations of the chromophore in its plane
3	$0_0 \rightarrow 7^1$	642	1.93	113	3245	0.378	Bending vibrations of the chromophore perpendicular to its plane
4	$0_0 \rightarrow 17^1$	634	1.96	312	9889	1.14	Compression-stretching of all four chromophore rings
5	$0_0 \rightarrow 32^1$	624	1.99	563	5117	0.580	
6	$0_0 \rightarrow 33^1$	623	1.99	573	2263	0.256	
7	$0_0 \rightarrow 34^1$	622	1.99	597	10880	1.23	
8	$0_0 \rightarrow 38^1$	620	2.00	665	3574	0.402	
9	$0_0 \rightarrow 64^1$	604	2.05	1083	5055	0.555	Vibrations of valence bonds and angles of the aminodiethyl group

λ is the wavelength, E is the transition energy, ν is the vibration frequency, I is the line intensity, and p is the dipole strength

Table 4. Calculated parameters of ground and excited electronic states and transitions between them in the visible region of the spectrum for NB in an aqueous solution

Electronic states	E_{eq}* (eV)	Electronic transition	λ_{adia} (nm)	E_{adia} (eV)	λ_{vert} (nm)	E_{vert} (eV)	λ_{vibron} (nm)	E_{vibron} (eV)	f	Involved transitions
S_0 (GS)	-27570.60									
S_1 (ES_1)	-27568.59	$S_0 \rightarrow S_1$	617	2.01	542	2.29	637	1.95	0.859	HOMO→LUMO
S_2 (ES_2)	-27567.97	$S_0 \rightarrow S_2$	471	2.63	435	2.85	533	2.33	0.0508	(HOMO-1)→LUMO
S_3 (ES_3)	-27567.53	$S_0 \rightarrow S_3$	404	3.07	371	3.34	471	2.63	0.0033	(HOMO-2)→LUMO

*equilibrium energy (PES minima, see Fig. 2)

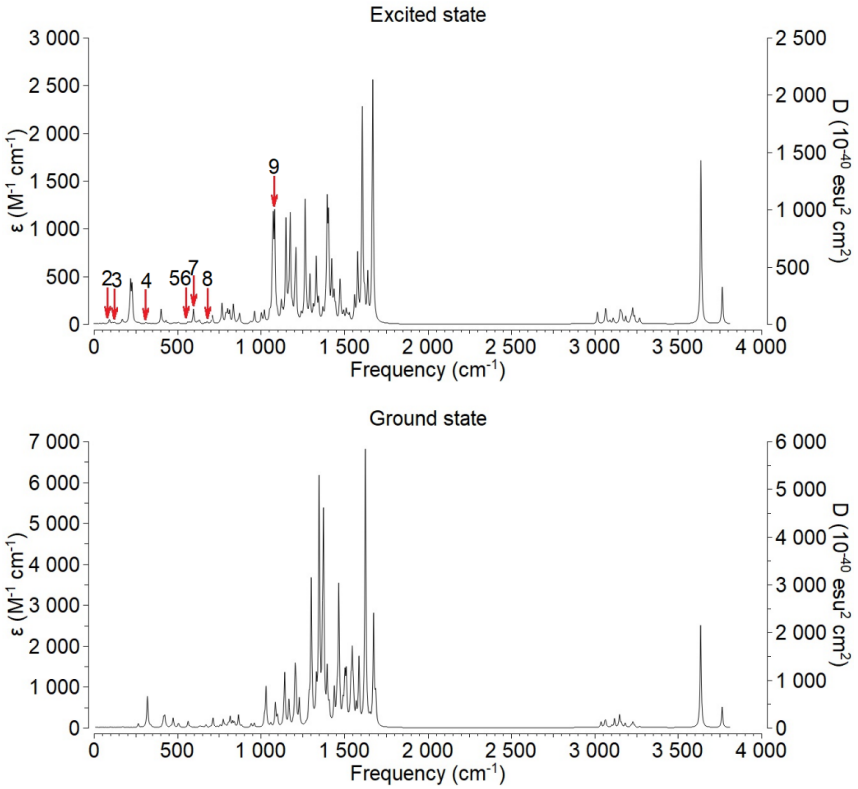

Figure 4. Calculated IR spectra of ground and first excited states of NB in aqueous solution. The peaks of the IR spectrum of the excited state, corresponding to the vibration frequencies involved in vibronic transitions (see Table 1), are shown by red arrows

The NB cation contains 168 electrons and, accordingly, 84 occupied molecular orbitals (MOs). The visualization of the frontier MOs involved in the considered electronic transition $S_0 \rightarrow S_1$ is shown in Fig. 5. Their configurations are close to the results from Refs. [103,105,106] calculated at the levels of the theory B3LYP/6-311++G(d,p), B3LYP/6-31G(d), and MS-CASPT2/ANO-LVDZP, respectively.

According to calculations, the dipole moment μ of the dye molecule almost does not change upon photoexcitation: $\mu_{GS} \approx \mu_{FC} \approx \mu_{ES} \approx 6$ D (Table 5) which contradicts the positive solvatochromism of NB. Therefore, it can be expected that the solvatochromism of NB is determined not by the dipole-dipole interaction with the solvent, but by site-specific contacts (hydrogen bonds) with it (see below). The μ values calculated by us are in satisfactory agreement with the values obtained in Refs. [26] (μ_{GS}=5.08 D), [78] (μ_{GS}=2.25 D, μ_{ES}=4.29 D (Lippert-Mataga); μ_{GS}=1.11 D, μ_{ES}=4.02 D (Bakshiev); μ_{GS}=1.65 D, μ_{ES}=6.19 D (Kawski-Chamma-Viallet)), [83] ($\Delta\mu=\mu_{ES} - \mu_{GS}$=2.9±1.5 D), [94] ($\mu_{GS}$=3.27 D), [105] ($\mu_{GS}$=4.94 D), but much less than the values calculated in Ref. [106] (μ_{GS}=20.7 D, μ_{FC}=18.2 D). Note that in Ref. [105] the value of the transition dipole moment M=4.98 D was obtained for NB at CPCM/B3LYP/6-311++G(d,p) theory level.

To understand the photoinduced charge redistribution in the NB molecule, we analyzed its Merz-Kollman [130] charges of heavy atoms in the ground and excited states. Upon photoexcitation, the shift of the electron density at immobile nuclei (transition to the Franck-Condon state) occurs mainly from the C10 atom to the N5 atom. Therefore, the μ_x component decreases even changing sign and μ_y component increases in absolute value, and, in general, the dipole moment μ of the molecule grows very slightly (see Table 4). The relaxation of NB to an equilibrium excited state by adjusting the coordinates of the nuclei to the excited configuration of the electron shells leads to an increase in the electron density on the C19 atom and its decrease on the C3 and C22 atoms. In turn, this causes a further decrease of μ_x, an increase

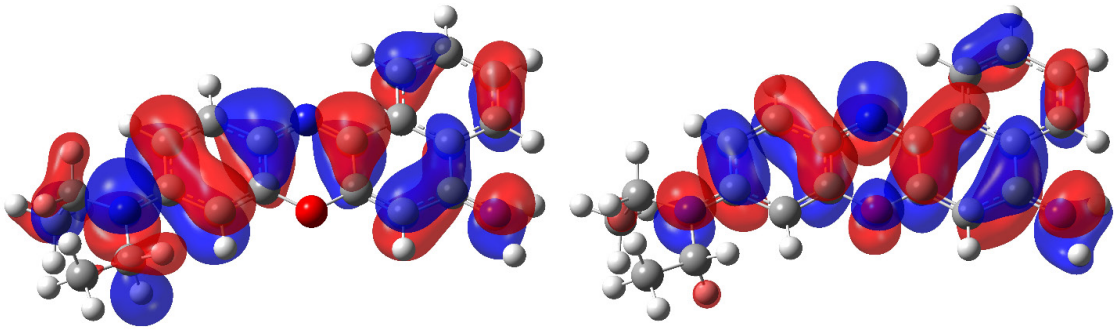

Figure 5. Frontier MOs, the transition between which corresponds to the main absorption peak in the visible region: HOMO (left) and LUMO (right). Positive lobes are shown in red and negative lobes in blue

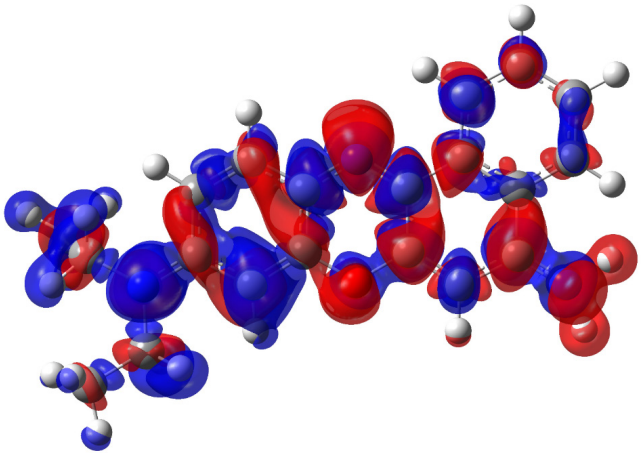

Figure 6. The electron density difference between Franck-Condon and ground states of NB cation. Regions of positive values are shown in red and negative values in blue

of the μ_y modulus, and an insignificant decrease in the total dipole moment μ of the cation. It should be noted that the redistribution of the electron density during the GS→FC vertical transition is much more significant than during the FC→ES relaxation (see Fig. 2).

Visualization of the difference in electron density (Fig. 6) shows that its photoinduced redistribution is complex and covers both the entire dye chromophore and side groups.

As you know, water is capable of forming strong hydrogen bonds with molecules of a solute. They are site-specific interactions that are considered in continuum models averaged only. To assess the effect of these hydrogen bonds on the photoexcitation of the NB molecule, we calculated the vibronic absorption spectrum for the "NB+4H_2O" hydrated complex (Fig. 7). All simulation parameters remained the same as in the calculations of the single cation NB described above.

Table 5. Calculated moments of NB cation in aqueous solution

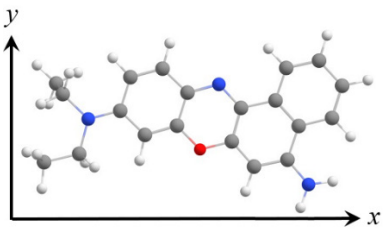

The coordinate axes are directed along the principal axes of inertia of the molecule

Dipole moment (D)	Ground state (S_0)	Excited state (S_1)		Ground to excited state transition dipole moment (D)	
		Franck-Condon (FC)	Equilibrium (ES)		
μ_x	2.02	-1.62	-1.28	M_x	13.5
μ_y	-5.70	-5.94	-6.02	M_y	-2.53
μ_z	0.326	0.341	0.0665	M_z	0.401
μ	6.06	6.17	6.16	M	13.8

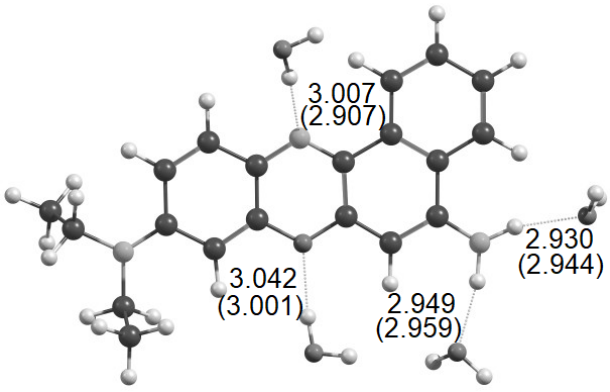

Figure 7. Calculated structure of the NB hydration complex with four water molecules. Strong hydrogen bonds are shown with a dotted line. Their lengths in Å (distances between heavy atoms) are given for the ground and equilibrium excited (in parentheses) states. A water molecule bound to the endocyclic nitrogen atom N5 is in front of the chromophore plane due to steric hindrances from the H9 and H15 atoms

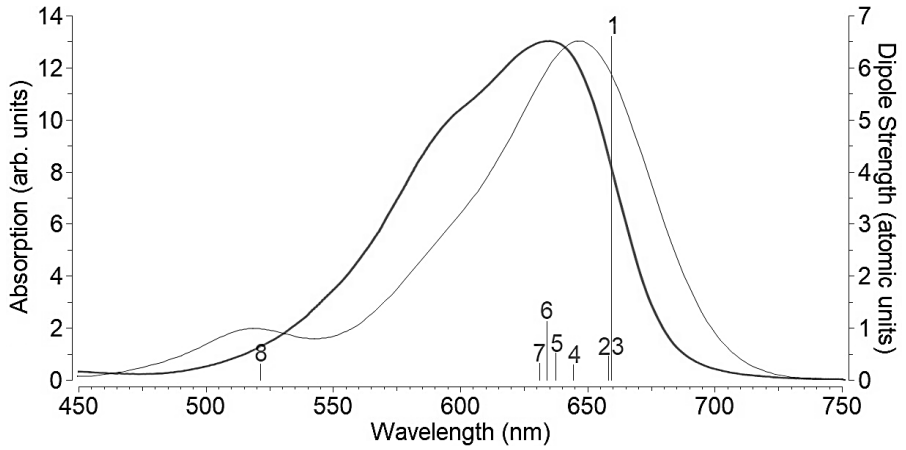

Figure 8. The calculated vibronic absorption spectrum of the "NB+4H_2O" system (thin line) and the experimental spectrum (2 μM NB in water) from Ref. [87] (thick line)

According to our calculations, two hydrogen bonds of NB chromophore with water in the excited state are stronger than in the ground state, which is manifested in their shortening. On the contrary, two bonds of the side amino group of the dye with water molecules are weakened by photoexcitation (see Fig. 7). The phenomenon of strengthening and weakening of hydrogen bonds with a solvent upon photoexcitation of various organic molecules was first discovered by Zhao and Han (see, for example, Ref. [131]). The vibronic absorption spectrum of the "NB+4H_2O" system, has the worst shape compared to a single NB cation. In this case, a small short-wavelength vibronic peak at ≈520 nm appears in the calculated spectrum, which is not observed in the experiment (Fig. 8). Besides, its absorption maximum is at λ_{vibron}=647 nm, the spectrum is redshifted by ≈10 nm. The absorption intensity has not changed (cf. Figs. 3 and 8).

Note that this pattern took place when calculating the energies of vertical transitions of proflavine in water [132]. Its explanation can be given as follows. Since the interaction with water molecules for NB in the excited state is stronger than in the ground state, the PES of the excited state drops lower than for a completely implicit specification of the aqueous environment (see Fig. 2). The convergence of the PESs of the ground and excited states leads to a decrease in E_{adia} and E_{vert} values, and, as a consequence, to an increase in λ_{vibron}.

It is of interest to analyze the effect of strong hydrogen bonds with water on the electronic and vibrational states of the dye. We note the changes in the vibronic transitions (cf. Figs. 4 and 9). Their number has decreased from 9 to 8, and the transitions themselves have changed significantly (cf. Tables 1 and S2). IR spectra (Fig. S6) and Duschinsky matrix (Fig. S7), respectively, also changed; in particular, the normal vibration modes of water molecules have been added. However, the configurations of the frontier orbitals (Fig. S8), electron density difference (Fig. 9), and electrostatic potential (Fig. S9) difference of the "NB+4H_2O" complex practically coincide with those for a single NB cation. It is interesting to note that out of four water molecules strongly bound to the OX4 cation, only one strongly polarizes upon excitation of the latter (bound to the N5 endocyclic nitrogen atom, see Fig. 9). As mentioned above, the electron density on this atom increases the most. This leads to a noticeable redistribution of the charge on the water molecule located nearby. This feature can also be seen on the corresponding electrostatic potential maps (Fig. S9 in Supplementary Material).

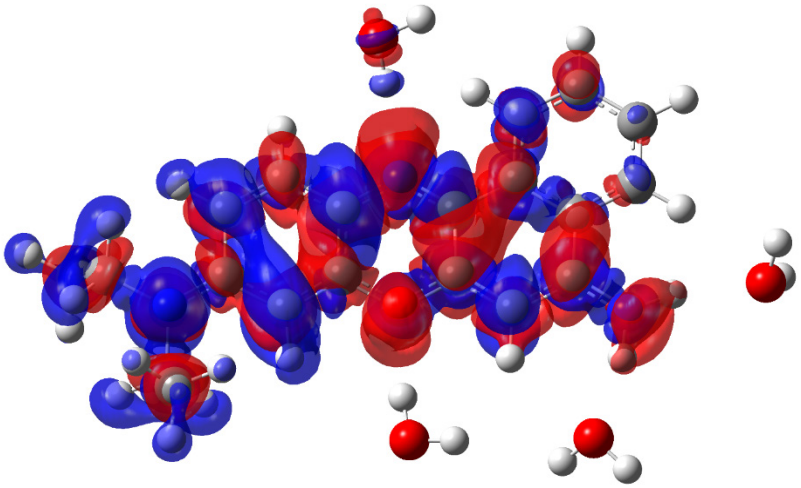

Figure 9. The electron density difference between Franck-Condon and ground states of the "NB+4H_2O" system

CONCLUSIONS

Of the 13 hybrid functionals used in this work to calculate the vibronic absorption spectrum of the NB dye in an aqueous solution, the best agreement with the experiment (λ_{max}=635 nm) in the position of the main maximum was given by O3LYP (λ_{vibron}=637 nm) with 6-31++G(d,p) basis set and IEFPCM solvent model. Vibronic coupling plays an important role in dye excitation. Thus, λ_{vibron} exceeds λ_{vert} by ~90 nm. The same shape is observed for vibronic spectra obtained using other functionals. Differences are observed in the position of the spectrum on the wavelength axis. Photoexcitation leads to changes in the vibrations, both in their frequencies and intensities. The dipole moment of the dye molecule in the ground state turned out to be almost the same as in the excited state. This result contradicts positive solvatochromism NB and means the important role of site-specific interactions (hydrogen bonds) in the solvatochromic behavior of the dye. Considering site-specific interactions in the form of an explicit assignment of four water molecules that form strong hydrogen bonds with the dye cation led to a redshift of the entire spectrum by ≈10 nm. At the same time, the shape of the spectrum worsened. A strengthening of two hydrogen bonds upon NB excitation was found, which explains the observed bathochromic effect from the nearest hydration shell of the dye.

References:

1. Jose M.J., Burgess K. Benzophenoxazine-based fluorescent dyes for labeling biomolecules. *Tetrahedron*, 2006, vol. 62, pp. 11021-11037.
2. Martinez V., Henary M. Nile Red and Nile Blue: Applications and Syntheses of Structural Analogues. *Chem. Eur. J.*, 2016, vol. 22, pp. 1-20.
3. Mohlau R., Uhlmann K. Zur kenntinss der chinazin- und oxazinfarbstoffe. *Ann. Chem.*, 1896, vol. 289, pp. 90-130.
4. Reichardt C. Solvatochromic Dyes as Solvent Polarity Indicators. *Chem. Rev.*, 1994, vol. 94, pp. 2319-2358.
5. Krihak M., Murtagh M., Shahriari M. A Spectroscopic Study of the Effects of Various Solvents and Sol-Gel Hosts on the Chemical and Photochemical Properties of Thionin and Nile Blue A. *J. Sol-Gel Sci. Technol.*, 1997, vol. 10, pp. 153-163.
6. Kobayashi T., Takagi Y., Kandori H., Kemnitz K., Yoshihara K. Femtosecond intermolecular electron transfer in diffusionless, weakly polar systems: nile blue in aniline and N,N-dimethylaniline. *Chem. Phys. Lett.*, 1991, vol. 180, pp. 416-422.
7. Woislawski S. The Spectrophotometric Determination of Ionization Constants of Basic Dyes. *J. Am. Chem. Soc.*, 1953, vol. 75, pp. 5201-5203.
8. Davis M.M., Helzer H.B. Titrimetric and Equilibrium Studies Using Indicators Related to Nile Blue A. *Anal. Chem.*, 1966, vol. 38, pp. 451-461.
9. Ma J., Ding C., Zhou J., Tian Y. 2D ratiometric fluorescent pH sensor for tracking of cells proliferation and metabolism. *Biosensors Bioelectronics*, 2015, vol. 70, pp. 202-208.
10. Lin C.-W., Shulok J.R., Kirley S.D., Cincotta L., Foley J.W. Lysosomal Localization and Mechanism of Uptake of Nile Blue Photosensitizers in Tumor Cells. *Cancer Res.*, 1991, vol. 51, pp. 2710-2719.
11. Mitra R.K., Sinha S.S., Maiti S., Pal S.K. Sequence Dependent Ultrafast Electron Transfer of Nile Blue in Oligonucleotides. *J. Fluoresc.*, 2009, vol. 19, pp. 353-361.
12. Huang C.Z., Li Y.F., Zhang D.J., Ao X.P., Spectrophotometric study on the supramolecular interactions of nile blue sulphate with nucleic acids. *Talanta*, 1999, vol. 49, pp. 495-503.
13. Chen Q.-Y., Li D.-H., Yang H.-H., Zhu Q.-Z., Xu J.-G., Zhao Y. Interaction of a novel red-region fluorescent probe, Nile Blue, with DNA and its application to nucleic acids assay. Analyst, 1999, vol. 124, pp. 901-906.
14. Huang C.Z., Li Y.F., Hu X.L. Three-dimensional spectra of the long-range assembly of Nile Blue sulfate on the molecular surface of DNA and determination of DNA by light-scattering. *Anal. Chim. Acta*, 1999, vol. 395, pp. 187-197.
15. Yang Y.-I., Hong H.-Y., Lee I.-S., Bai D.-G., Yoo G.-S., Choi J.-K. Detection of DNA Using a Visible Dye, Nile Blue, in Electrophoresed Gels. *Anal. Biochem.*, 2000, vol. 280, pp. 322-324.
16. Alipour E., Allaf F.N., Mahmoudi-Badiki T. Investigation of specific interactions between Nile blue and single type oligonucleotides and its application in electrochemical detection of hepatitis C3a virus. *J. Solid State Electrochem.*, 2016, vol. 20, pp. 183-192.
17. Mindroiu M., Zgarian R.G., Kajzar F., Rau I., De Oliveira H.C.L., Pawlicka A., Tihan G.T. DNA-based membranes for potential applications. *Ionics*, 2015, vol. 21, pp. 1381-1390.
18. Sagara T., Igarashi S., Sato H., Niki K. Voltammetric application of electromodulated electroreflection absorption spectroscopy: electroreflectance voltammetry as an in situ spectroelectrochemical technique. *Langmuir*, 1991, vol. 7, pp. 1005-1012.
19. Wainwright M. Non-porphyrin photosensitizers in biomedicine. *Chem. Soc. Rev.*, 1996, vol. 25, pp. 351-359.
20. Van Staveren H.J., Speelman O.C., Witjes M.J., Cincotta L., Star W.M. Fluorescence imaging and spectroscopy of ethyl nile blue a in animal models of (pre)malignancies. *Photochem. Photobiol.*, 2001, vol. 73, pp. 32-38.
21. Lin C.-W., Shulok J.R., Wong Y.-K., Schanbacher C.F., Cincotta L., Foley J.W. Photosensitization, Uptake, and Retention of Phenoxazine Nile Blue Derivatives in Human Bladder Carcinoma Cells. *Cancer Res.*, 1991, vol. 51, pp. 1109-1116.
22. Vecchio D., Bhayana B., Huang L., Carrasco E., Evans C.L., Hamblin M.R. Structure-function relationships of Nile blue (EtNBS) derivatives as antimicrobial photosensitizers. *Eur. J. Med. Chem.*, 2014, vol. 75, pp. 479-491.

23. Hirakawa K., Ota K., Hirayama J., Oikawa S., Kawanishi S. Nile Blue Can Photosensitize DNA Damage through Electron Transfer. *Chem. Res. Toxicol*., 2014, vol. 27, pp. 649-655.

24. Gattuso H., Besancenot V., Grandemange S., Marazzi M., Monari A. From non-covalent binding to irreversible DNA lesions: nile blue and nile red as photosensitizing agents. *Sci. Rep*., 2016, vol. 6, p. 28480.

25. Huang M., He S., Liu W., Yao Y., Miao S. Spectral Inspections on Molecular Configurations of Nile Blue A Adsorbed on the Elementary Clay Sheets. *J. Phys. Chem. B*, 2015, vol. 119, pp. 13302-13308.

26. Gilani A.G., Moghadam M., Hosseini S.E., Zakerhamidi M.S. A comparative study on the aggregate formation of two oxazine dyes in aqueous and aqueous urea solutions. *Spectrochim. Acta A*, 2011, vol. 83, pp. 100-105.

27. Niazi A., Yazdanipour A., Ghasemi J., Kubista M. Spectrophotometric and thermodynamic study on the dimerization equilibrium of ionic dyes in water by chemometrics method. *Spectrochim. Acta A*, 2006, vol. 65, pp. 73-78.

28. Goftar M.K., Moradi K., Kor N.M. Spectroscopic studies on aggregation phenomena of dyes. *Eur. J. Exp. Biol*., 2014, vol. 4, pp. 72-81.

29. Antonov L., Gergov G., Petrov V., Kubista M., Nygren J. UV–Vis spectroscopic and chemometric study on the aggregation of ionic dyes in water. *Talanta*, 1999, vol. 49, pp. 99-106.

30. Chakraborty A., Adhikari R., Saha S.K. Molecular interaction of oxazine dyes in aqueous solution: Temperature dependent molecular disposition of the aggregates. *J. Mol. Liquids*, 2011, vol. 164, pp. 250-256.

31. Ghanadzadeh Gilani A., Shokri S. Spectral and aggregative properties of two oxazine dyes in aqueous solutions containing structure-breaking and multifunctional additives. *J. Mol. Liquids*, 2014, vol. 193, pp. 194-203.

32. Hazafy D., Salvia M.-V., Mills A., Hutchings M.G., Evstigneev M.P., Parkinson J.A. NMR analysis of Nile Blue (C. I. Basic Blue 12) and Thionine (C. I. 52000) in solution. *Dyes Pigments*, 2011, vol. 88, pp. 315-325.

33. Nasr A., Hotchandani S. Excited-State Behavior of Nile Blue H-Aggregates Bound to SiO2 and SnO2 Colloids. *Chem. Mater*., 2000, vol. 12, pp. 1529-1535.

34. Mishra S.S., Subuddhi U. Spectroscopic investigation of interaction of Nile Blue A, a potent photosensitizer, with bile salts in aqueous medium. *J. Photochem. Photobiol. B*, 2014, vol. 141, pp. 67-75.

35. Chubinidze K., Partsvania B., Sulaberidze T., Khuskivadze A., Davitashvili E., Koshoridze N. Luminescence enhancement in nanocomposite consisting of polyvinyl alcohol incorporated gold nanoparticles and Nile blue 690 perchlorate. *Appl. Optics*, 2014, vol. 53, pp. 7177-7181.

36. Fan J., Dong H., Hu M., Wang J., Zhang H., Zhu H., Sun W., Peng X. Fluorescence imaging lysosomal changes during cell division and apoptosis observed using Nile Blue based near-infrared emission. *Chem. Commun*., 2014, vol. 50, pp. 882-884.

37. Lee S.H., Suh J.K., Li M. Determination of Bovine Serum Albumin by Its Enhancement Effect of Nile Blue Fluorescence. *Bull. Korean Chem. Soc*., 2003, vol. 24, pp. 45-48.

38. Kuramitz H., Piruska A., Halsall H.B., Seliskar C.J., Heineman W.R. Simultaneous Multiselective Spectroelectrochemical Sensing of the Interaction between Protein and Its Ligand Using the Redox Dye Nile Blue as a Label. *Anal. Chem*., 2008, vol. 80, pp. 9642-9648.

39. Mitra R.K., Sinha S.S., Pal S.K. Interactions of Nile Blue with Micelles, Reverse Micelles and a Genomic DNA. *J. Fluoresc*., 2008, vol. 18, pp. 423-432.

40. Das K., Jain B., Patel H.S. Nile Blue in Triton-X 100/benzene-hexane reverse micelles: a fluorescence spectroscopic study. *Spectrochim. Acta A*, 2004, vol. 60, pp. 2059-2064.

41. Dong J., Li Y., Zhang M., Li Z., Yan T., Qian W. Ultrasensitive surface-enhanced Raman scattering detection of alkaline phosphatase. *Anal. Methods*, 2014, vol. 6, pp. 9168-9172.

42. Wilson A.J., Willets K.A. Unforeseen distance-dependent SERS spectroelectrochemistry from surface-tethered Nile Blue: the role of molecular orientation. *Analyst*., 2016, vol. 141, pp. 5144-5151.

43. Reigue A., Auguie B., Etchegoina P.G., Le Ru E.C. CW measurements of resonance Raman profiles, line-widths, and cross-sections of fluorescent dyes: application to Nile Blue A in water and ethanol. *J. Raman Spectrosc*., 2013, vol. 44, pp. 573-581.

44. Esmaeili B., Heng L.Y., Ling T.L. Nile Blue chromoionophore-doped kappa-carrageenan for a novel reflectometric urea biosensor. *Sensors Actuators B*, 2015, vol. 221, pp. 969-977.

45. Madsen J., Canton I., Warren N.J., Themistou E., Blanazs A., Ustbas B., Tian X., Pearson R., Battaglia G., Lewis A.L., Armes S.P. Nile Blue-Based Nanosized pH Sensors for Simultaneous Far-Red and Near-Infrared Live Bioimaging. *J. Am. Chem. Soc*., 2013, vol. 135, pp. 14863-14870.

46. Gao Y.-S., Zhu X.-F., Xu J.-K., Lu L.-M., Wang W.-M., Yang T.-T., Xing H.-K., Yu Y.-F. Label-free electrochemical immunosensor based on Nile blue A-reduced graphene oxide nanocomposites for carcinoembryonic antigen detection. *Anal. Biochem*., 2016, vol. 500, pp. 80-87.

47. Jin H., Zhao C., Gui R., Gao X., Wang Z. Reduced graphene oxide/nile blue/gold nanoparticles complex-modified glassy carbon electrode used as a sensitive and label-free aptasensor for ratiometric electrochemical sensing of dopamine. *Anal. Chim. Acta*, 2018, vol. 1025, pp. 154-162.

48. Duan R., Li C., Liu S., Liu Z., Li Y., Zhu J., Hu X. A selective fluorescence quenching method for the determination of trace hypochlorite in water samples with nile blue A. *J. Taiwan Inst. Chem. Eng*., 2015, vol. 50, pp. 43-48.

49. Chen Q., Cheng Z., Du L., Zhu P., Tan K. A sensitive three-signal assay for the determination of PFOS based on the interaction with Nile blue A. *Anal. Methods*, 2018, vol. 10, pp. 3052-3058.

50. Lee M.H., Lee S.W., Kim S.H., Kang C., Kim J.S. Nanomolar Hg(II) Detection Using Nile Blue Chemodosimeter in Biological Media. *Org. Lett*., 2009, vol. 11, pp. 2101-2104.

51. Li Z., Wang J., Xu Q. Spectrophotometric Determination of Trace Amounts of Scandium with Molybdate, Nile Blue and Poly(vinyl alcohol). *Anal. Sci*., 1996, vol. 12, pp. 259-262.

52. Hu M., Yin J., Li Y., Zhao X. Development of a Nile-Blue Based Chemodosimeter for Hg2+ in Aqueous Solution and its Application in Biological Imaging. *J. Fluoresc*., 2015, vol. 25, pp. 403-408.

53. Gao H.-W., Ye Q.-S., Liu W.-G. Langmuir Aggregation of Nile Blue and Safranine T on Sodium Dodecylbenzenesulfonate Surface and Its Application to Quantitative Determination of Anionic Detergent. *Anal. Sci*., 2002, vol. 18, pp. 455-459.

54. Basting A., Ouw D., Schafer F.P. The phenoxazones: A new class of laser dyes. *Optics Commun*., 1976, vol. 18, pp. 260-262.

55. Siami A., Sabzi R.E., Rasouli F., Kheiri F. Nile Blue and Nickel Organometallic Dyes Applied in Dye-sensitized Solar Cells. *Port. Electrochim. Acta*, 2015, vol. 33, pp. 23-33.

56. Bancroft J.D., Cook H.C. *Manual of Histological Techniques and their Diagnostic Application*. Churchill Livingstone, Edinburgh, 1994.

57. Betscheider A., Jose J. Nile blue A for staining Escherichia coli in flow cytometer experiments. *Anal. Biochem*., 2009, vol. 384, pp. 194-196.

58. Frick A.A., Busetti F., Cross A., Lewis S.W. Aqueous Nile Blue: A Simple, Versatile and Safe Reagent for the Detection of Latent Fingermarks. *Chem. Commun*., 2014, vol. 50, pp. 3341-3343.

59. Shrivastava R., Jain B., Das K. Spectroscopic investigations on the binding of Methylene Blue and Nile Blue to negatively charged gold nanorods. *J. Mol. Struct*., 2012, vol. 1020, pp. 56-62.

60. Wilson A.J., Molina N.Y., Willets K.A. Modification of the Electrochemical Properties of Nile Blue through Covalent Attachment to Gold as Revealed by Electrochemistry and SERS. *J. Phys. Chem. C*, 2016, vol. 120, pp. 21091-21098.

61. Marowsky A., Gierulski A., Dick B. Double-resonant second harmonic generation from surface coverages of Nile Blue A. *Optics Commun*., 1985, vol. 52, pp. 339-342.

62. Craighead H.G., Glass A.M. Optical absorption of small metal particles with adsorbed dye coats. *Optics Lett*., 1981, vol. 6, pp. 248-250.

63. Baigar E., Gilch P., Zinth W., Stockl M., Harter P., von Feilitzsch T., Michel-Beyerle M.E. Ultrafast intramolecular electron transfer from a ferrocene donor moiety to a nile blue acceptor. *Chem. Phys. Lett*., 2002, vol. 352, pp. 176-184.

64. Shervedani R.K., Amini S.A. Preparation of graphene/nile blue nanocomposite: Application for oxygen reduction reaction and biosensing. *Electrochim. Act*., 2015, vol. 173, pp. 354-363.

65. Peng J.-J., Liu S.-P., Wang L., He Y.-Q. Studying the interaction between CdTe quantum dots and Nile blue by absorption, fluorescence and resonance Rayleigh scattering spectra. *Spectrochim. Acta A*, 2010, vol. 75, pp. 1571-1576.

66. Shen Y., Liu S., Kong L., Tan X., He Y., Yang J. Detection of DNA using an “off-on” switch of a regenerating biosensor based on an electron transfer mechanism from glutathione-capped CdTe quantum dots to nile blue. Analyst, 2014, vol. 139, pp. 5858-5867.

67. Al-Maliki A. Energy transfer studies in binary laser dye mixtures in organically modified silicates. *Eur. Phys. J. D*., 2014, vol. 68, p. 236.

68. Jose J., Ueno Y., Burgess K. Water-Soluble Nile Blue Derivatives: Syntheses and Photophysical Properties. *Chem. Eur. J*., 2009, vol. 15, pp. 418-423.

69. Liu X., Fan C., Sun R., Ge J.-F. Nile-red and Nile-blue-based near-infrared fluorescent probes for in-cellulo imaging of hydrogen sulfide. *Anal. Bioanal. Chem*., 2014, vol. 406, pp. 7059-7070.

70. Raju B.R., Naik S., Coutinho P.J.G., Goncalves M.S.T. Novel Nile Blue derivatives as fluorescent probes for DNA. *Dyes Pigments*, 2013, vol. 99, pp. 220-227.

71. Ho N.-H., Weissleder R., Tung C.-H. Development of water-soluble far-red fluorogenic dyes for enzyme sensing. Tetrahedron, 2006, vol. 62, pp. 578-585.

72. Raju B.R., Sampaio D.M.F., Silva M.M., Coutinho P.J.G., Goncalves M.S.T. Ultrasound promoted synthesis of Nile Blue derivatives. *Ultrasonics Sonochem*., 2014, vol. 21, pp. 360-366.

73. Basu S., Panigrahi S., Praharaj S., Ghosh S.K., Pande S., Jana S., Pal A., Pal T. Solvent Effect on the Electronic Spectra of Azine Dyes under Alkaline Condition. *J. Phys. Chem. A*, 2007, vol. 111, pp. 578-583.

74. Grofcsik A., Kubinyi M., Jones W. Intermolecular photoinduced proton transfer in nile blue and oxazine 720. *Chem. Phys. Lett*., 1996, vol. 250, pp. 261-265.

75. Douhal A. Photophysics of Nile Blue A in Proton-Accepting and Electron-Donating Solvents. *J. Phys. Chem*., 1994, vol. 98, pp. 13131-13137.

76. Kandori A., Kemnitz K., Yoshihara K. Subpicosecond transient absorption study of intermolecular electron transfer between solute and electron-donating solvents. *J. Phys. Chem*., 1992, vol. 96, pp. 8042-8048.

77. Lakowicz J.R., Zelent B., Kusba J., Gryczynski I. Distance-dependent quenching of Nile Blue fluorescence by N,N-diethylaniline observed by frequency-domain fluorometry. *J. Fluoresc*., 1996, vol. 6, pp. 187-194.

78. Gilani A.G., Hosseini S.E., Moghadam M., Alizadeh E. Excited state electric dipole moment of nile blue and brilliant cresyl blue: A comparative study. *Spectrochim. Acta A*, 2012, vol. 89, pp. 231-237.

79. Tajalli A., Gilani A.G., Zakerhamidi M.S., Tajalli P. The photophysical properties of Nile red and Nile blue in ordered anisotropic media. *Dyes Pigments*, 2008, vol. 78, pp. 15-24.

80. Ghanadzadeh A., Tajalli H., Zirack P., Shirdel J. On the photo-physical behavior and electro-optical effect of oxazine dyes in anisotropic host. *Spectrochim. Acta A*, 2004, vol. 60, pp. 2925-2932.

81. Wang X.-L., Sun R., Zhu W.-J., Sha X.-L., Ge J.-F. Reversible Absorption and Emission Responses of Nile Blue and Azure A Derivatives in Extreme Acidic and Basic Conditions. *J. Fluoresc*., 2017, vol. 27, pp. 819-827.

82. Stockett M.H., Houmoller J., Nielsen S.B. Nile blue shows its true colors in gas-phase absorption and luminescence ion spectroscopy. *J. Chem. Phys*., 2016, vol. 145, p. 104303.

83. Beuerman E., Makarov N.S., Drobizhev M., Rebane A. Justification of two-level approximation for description of two-photon absorption in Oxazine dyes. *Proc. SPIE*, 2010, vol. 7599, p. 75990X.

84. Blau W., Dankesreiter W., Penzkofer A. Saturable absorption of dyes excited to the long-wavelength region of the S0-S1 absorption band. *Chem. Phys*., 1984, vol. 85, pp. 473-479.

85. Fragnito H.L., Bigot J.-Y., Becker P.C., Shank C.V. Evolution of the vibronic absorption spectrum in a molecule following impulsive excitation with a 6 fs optical pulse. *Chem. Phys. Lett*., 1989, vol. 160, pp. 101-104.

86. Pollard W.T., Fragnito H.L., Bigot J.-Y., Shank C.V., Mathies R.A. Quantum-mechanical theory for 6 fs dynamic absorption spectroscopy and its application to nile blue. *Chem. Phys. Lett*., 1990, vol. 168, pp. 239-245.

87. Steinhurst D.A., Owrutsky J.C. Second Harmonic Generation from Oxazine Dyes at the Air/Water Interface. *J. Phys. Chem. B*, 2001, vol. 105, pp. 3062-3072.

88. Sens R., Drexhage K.H. Fluorescence quantum yield of oxazine and carbazine laser dyes. *J. Luminesc*, 1981, vol. 24-25, pp. 709-712.

89. Zhang Y., Hartmann S.R. Fluorescence-line-narrowing spectroscopy of nile blue in glass and polymer at 5 K: Determination of a single-site line shape function. *J. Chem. Phys*., 1996, vol. 104, pp. 4371-4379.

90. Grofcsik A., Jones W.J. Stimulated emission cross-sections in fluorescent dye solutions: gain spectra and excited-state lifetimes of Nile blue A and oxazine 720. *J. Chem. Soc., Faraday Trans*., 1992, vol. 88, pp. 1101-1106.

91. Moshary F., Arend M., Friedberg R., Hartmann S.R. Ultrafast relaxation and modulation in the oxazine dye nile blue. *Phys. Rev. A*, 1992, vol. 46, pp. 33-36.

92. Weiner A.M., Ippen E.P. Femtosecond excited state relaxation of dye molecules in solution. *Chem. Phys. Lett*., 1985, vol. 114, pp. 456-460.

93. Taylor A.J., Erskine D.J., Tang C.L. Femtosecond vibrational relaxation of large organic molecules. *Chem. Phys. Lett*., 1984, vol. 103, pp. 430-435.

94. Kubinyi M., Grofcsik A., Papai I., Jones W.J. Rotational reorientation dynamics of nile blue A and oxazine 720 in protic solvents. *Chem. Phys*., 2003, vol. 286, pp. 81-96.

95. Lawless M.K., Mathies R.A. Excited-state structure and electronic dephasing time of Nile blue from absolute resonance Raman intensities. *J. Chem. Phys*., 1992, vol. 96, pp. 8037-8045.

96. Egorova D., Gelin M.F., Domcke W. Analysis of vibrational coherences in homodyne and two-dimensional heterodyne photon-echo spectra of Nile Blue. *Chem. Phys*., 2007, vol. 341, pp. 113-122.

97. Prall B.S., Parkinson D.Y., Fleming G.R. Probing correlated spectral motion: Two-color photon echo study of Nile blue. *J. Chem. Phys*., 2005, vol. 123, p. 054515.

98. Nagasawa Y., Seike K., Muromoto T., Okada T. Two-Dimensional Analysis of Integrated Three-Pulse Photon Echo Signals of Nile Blue Doped in PMMA. *J. Phys. Chem. A*, 2003, vol. 107, pp. 2431-2441.

99. Brixner T., Mancal T., Stiopkin I.V., Fleming G.R. Phase-stabilized two-dimensional electronic spectroscopy. *J. Chem. Phys*., 2004, vol. 121, pp. 4221-4236.

100. Ali Q.M., Palanisamy P.K. Z-Scan Determination of the Third-Order Optical Nonlinearity of Organic Dye Nile Blue Chloride. *Modern Phys. Lett. B*, 2006, vol. 20, pp. 623-632.

101. Blanchard G.J. An MNDO calculational study of selected oxazine, thiazine and oxazone dyes. *Chem. Phys*., 1989, vol. 138, pp. 365-375.

102. Pollard W.T., Fragnito H.L., Bigot J.-Y., Shank C.V., Mathies R.A. Quantum-mechanical theory for 6 fs dynamic absorption spectroscopy and its application to nile blue. *Chem Phys Lett*, 1990, vol. 168, pp. 239-245.

103. Grofcsik A., Kubinyi M., Ruzsinszky A., Veszpremi T., Jones W.J. Quantum chemical studies on excited state intermolecular proton transfer of oxazine dyes. *J. Mol. Structure*, 2000, vol. 555, pp. 15-19.

104. Cossi M., Rega N., Scalmani G., Barone V. Energies, structures, and electronic properties of molecules in solution with the C-PCM solvation model. *J. Comp. Chem*., 2003, vol. 24, pp. 669-681.

105. Fleming S., Mills A., Tuttle T. Predicting the UV–vis spectra of oxazine dyes. *Beilstein J. Org. Chem*., 2011, vol. 7, pp. 432-441.

106. Marazzi M., Gattuso H., Monari A. Nile blue and Nile red optical properties predicted by TD-DFT and CASPT2 methods: static and dynamic solvent effects. *Theor. Chem. Acc*., 2016, vol. 135, p. 57.

107. Adamo C., Jacquemin D. The calculations of excited-state properties with Time-Dependent Density Functional Theory. *Chem. Soc. Rev*., 2013, vol. 42, pp. 845-856.

108. Charaf-Eddin A., Planchat A., Mennucci B., Adamo C., Jacquemin D. Choosing a Functional for Computing Absorption and Fluorescence Band Shapes with TD-DFT. *J. Chem. Theory Comput*., 2013, vol. 9, pp. 2749-2760.

109. Condon E.U. Nuclear motions associated with electron transitions in diatomic molecules. *Phys. Rev*., 1928, vol. 32, pp. 858-872.

110. Baiardi A., Bloino J., Barone V. General Time Dependent Approach to Vibronic Spectroscopy Including Franck-Condon, Herzberg-Teller, and Duschinsky Effects. *J. Chem. Theory Comput*., 2013, vol. 9, pp. 4097-4115.

111. Frisch M.J., Trucks G.W., Schlegel H.B. et al. *Gaussian 16*. Revision C.01, Inc., Wallingford CT, 2016.

112. Herzberg G., Teller E. Schwingungsstruktur der Elektronenubergange bei mehratomigen Molekulen. *Z. Phys. Chem., Abt. B*, 1933, vol. 21, pp. 410-446.

113. Santoro F., Lami A., Improta R., Bloino J., Barone V. Effective method for the computation of optical spectra of large molecules at finite temperature including the Duschinsky and Herzberg-Teller effect: The Qx band of porphyrin as a case study. *J. Chem. Phys*., 2008, vol. 128, p. 224311.

114. Duschinsky F. The importance of the electron spectrum in multi atomic molecules. Concerning the Franck-Condon principle. *Acta Physicochim. URSS*, 1937, vol. 7, p. 551.

115. Scalmani G., Frisch M.J. Continuous surface charge polarizable continuum models of solvation. I. General formalism. *J. Chem. Phys*., 2010, vol. 132, p. 114110.

116. Improta R., Scalmani G., Frisch M.J., Barone V. Toward effective and reliable fluorescence energies in solution by a new State Specific Polarizable Continuum Model Time Dependent Density Functional Theory Approach. *J. Chem. Phys*., 2007, vol. 127, p. 074504.

117. Jacquemin D., Bremond E., Planchat A., Ciofini I., Adamo C. TD-DFT vibronic couplings in anthraquinones: from basis set and functional benchmarks to applications for industrial dyes. *J. Chem. Theory Comput*., 2011, vol. 7, pp. 1882-1892.

118. Barboza C.A., Vazquez P.A.M., Carey D.M.-L., Arratia-Perez R. A TD-DFT Basis Set and Density Functional Assessment for the Calculation of Electronic Excitation Energies of Fluorene. *Int. J. Quant. Chem*., 2012, vol. 112, pp. 3434-3438.

119. Jacquemin D., Bremond E., Ciofini I., Adamo C. Impact of Vibronic Couplings on Perceived Colors: Two Anthraquinones as a Working Example. *J. Phys. Chem. Lett*., 2012, vol. 3, pp. 468-471.

120. Lopez G.V., Chang C.-H., Johnson P.M., Hall G.E., Sears T.J., Markiewicz B., Milan M., Teslja A. What Is the Best DFT Functional for Vibronic Calculations? A Comparison of the Calculated Vibronic Structure of the S1−S0 Transition of Phenylacetylene with Cavity Ringdown Band Intensities. *J. Phys. Chem. A*, 2012, vol. 116, pp. 6750-6758.

121. Dierksen M., Grimme S. The Vibronic Structure of Electronic Absorption Spectra of Large Molecules: A Time-Dependent Density Functional Study on the Influence of "Exact" Hartree-Fock Exchange. *J. Phys. Chem. A*, 2004, vol. 108, pp. 10225-10237.

122. Kantchev E.A.B., Norsten T.B., Sullivan M.B. Time-dependent density functional theory (TDDFT) modelling of Pechmann dyes: from accurate absorption maximum prediction to virtual dye screening. *Org. Biomol. Chem*., 2012, vol. 10, pp. 6682-6692.

123. Tawada Y., Tsuneda T., Yanagisawa S., Yanai T., Hirao K. A long-range-corrected time-dependent density functional theory. *J. Chem. Phys*., 2004, vol. 120, pp. 8425-8433.

124. Rostov I.V., Kobayashi R., Amos R.D. Comparing long-range corrected functionals in the cis–trans isomerisation of the retinal chromophore. *Mol. Phys*., 2012, vol. 110, pp. 2329-2336.

125. Dreuw A., Weisman J.L., Head-Gordon M. Long-range charge-transfer excited states in time-dependent density functional theory require non-local exchange. *J. Chem. Phys*., 2003, vol. 119, pp. 2943-2946.

126. Chiba M., Tsuneda T., Hirao K. Long-range corrected time-dependent density functional study on fluorescence of 4,4'-dimethylaminobenzonitrile. *J. Chem. Phys*., 2007, vol. 126, p. 034504.

127. Dennington R., Keith T.A., Millam J.M. *GaussView*, Version 6.1, Semichem Inc., Shawnee Mission KS, 2016.

128. Cohen A.J., Handy N.C. Dynamic correlation. *Mol. Phys*., 2001, vol. 99, pp. 607-615.

129. Marenich A.V., Cramer C.J., Truhlar D.G. Universal solvation model based on solute electron density and a continuum model of the solvent defined by the bulk dielectric constant and atomic surface tensions. *J. Phys. Chem. B*, 2009, vol. 113, pp. 6378-6396.

130. Singh U.C., Kollman P.A. An approach to computing electrostatic charges for molecules, *J. Comput. Chem.*, 1984, vol. 5, pp. 129-145.

131. Zhao G.J., Han K.L. Effects of hydrogen bonding on tuning photochemistry: Concerted hydrogen-bond strengthening and weakening. *ChemPhysChem*, 2008, vol. 9, pp. 1842-1846.

132. Qin Z., Lib X., Zhou M. A Theoretical Study on Hydrogen-Bonded Complex of Proflavine Cation and Water: The Site-dependent Feature of Hydrogen Bond Strengthening and Weakening. *J. Chin. Chem. Soc*., 2014, vol. 61, pp. 1199-1204.